Sea ice loss enhances wave action at the Arctic coast

Irina Overeem,[1] Robert S. Anderson,[1,2] Cameron W. Wobus,[3,4] Gary D. Clow,[5] Frank E. Urban,[5] and Nora Matell[1]

Received 26 June 2011; revised 12 August 2011; accepted 13 August 2011; published 9 September 2011.

[1] Erosion rates of permafrost coasts along the Beaufort Sea accelerated over the past 50 years synchronously with Arctic-wide declines in sea ice extent, suggesting a causal relationship between the two. A fetch-limited wave model driven by sea ice position and local wind data from northern Alaska indicates that the exposure of permafrost bluffs to seawater increased by a factor of 2.5 during 1979–2009. The duration of the open water season expanded from ~45 days to ~95 days. Open water expanded more rapidly toward the fall (~0.92 day yr^{-1}), when sea surface temperatures are cooler, than into the mid-summer (~0.71 days yr^{-1}).Time-lapse imagery demonstrates the relatively efficient erosive action of a single storm in August. Sea surface temperatures have already decreased significantly by fall, reducing the potential impact of thermal erosion due to fall season storm waves.
Citation: Overeem, I., R. S. Anderson, C. W. Wobus, G. D. Clow, F. E. Urban, and N. Matell (2011), Sea ice loss enhances wave action at the Arctic coast, *Geophys. Res. Lett.*, *38*, L17503, doi:10.1029/2011GL048681.

1. Introduction

[2] More than any other region on Earth, the Arctic is responding to climate change: temperatures have warmed at almost twice the global rate [*Serreze et al.*, 2000], the Arctic Ocean has warmed [*Steele et al.*, 2008], permafrost is thawing [*Clow*, 2008; *Smith et al.*, 2010], and sea ice extent has been decreasing, with especially high rates in the Beaufort Sea and Chukchi Sea [*Serreze et al.*, 2007; *Stroeve et al.*, 2008]. Concurrently, already high coastal erosion rates [*Solomon et al.*, 1994; *Are et al.*, 2008] appear to be accelerating along permafrost coastlines of the Alaskan Beaufort Sea and the Yukon Coast [*Mars and Houseknecht*, 2007; *Jones et al.*, 2009; *Lantuit and Pollard*, 2008]. Documentation of erosion rates from aerial photos along a 75 km stretch of the Alaskan Beaufort Sea reveals that the mean annual erosion rates doubled from ~7 m yr^{-1} for 1955–1979 to ~14 m yr^{-1} for 2002–2007 [*Jones et al.*, 2009]. We measured an average retreat of 14.4 m yr^{-1} over a 3 km stretch of coast in the two-year interval 2007–2009, with rates as high as 30 m yr^{-1} locally [*Wobus et al.*, 2011]. Arctic coastal communities are affected by such rapid land loss, and petroleum infrastructure in the National Petroleum Reserve-Alaska is locally at risk of being lost to coastal erosion [*Holland-Bartels and Pierce*, 2011], and the contribution of Carbon from coastal bluffs to the ocean is accelerated [*Ping et al.*, 2011].

[3] Although the circumstantial evidence is strong that the observed acceleration in coastal erosion rates is related to ongoing climate change, the mechanisms that govern this change have yet to be fully quantified. In this study we focus on those reaches of permafrost coastline that consist of 2–5 m high ice-rich, silty bluffs and drained thaw lakes, spanning ~480 km along the Beaufort Sea [*Ping et al.*, 2011]. Notches several meters deep are melted into the ice-rich permafrost just above sea level when relatively warm water bathes their base during the sea ice-free ("open water") season [*Kobayashi*, 1985]. Blocks eventually topple when the notch is deep enough to destabilize them [*Hoque and Pollard*, 2009]. However, even during the open water season, our field observations indicate that the rate of undercutting is limited by the ability of relatively warm seawater to access the bluffs, and melt the interstitial ice that binds them [*Wobus et al.*, 2011]. This is in turn controlled by the water surface elevation and wave height. In this study, we focus on modeling the interactions among the evolving sea ice margin, the nearshore sea ice concentration, and the storm climate to predict the fetch-limited, shallow-water wave field and quantify changes in these parameters through time.

2. Modeling of Nearshore Processes

2.1. Sea Ice Dynamics

[4] We used Nimbus 7-SMMR/SSM/I and DMSP SSMI Passive Microwave data to assess daily sea ice concentration near Drew Point (70.877N, 153.936W) along the Beaufort Sea. Sea Ice Concentrations (SIC) are derived from brightness temperature data and are available from the National Snow and Ice Data Center, (NSIDC, http://nsidc.org/data/nsidc-0051.html). While this Arctic-wide dataset is the longest continuous record of sea ice and covers 1979 to 2009 at daily or bi-daily temporal resolution, it suffers from a low spatial resolution (~25 × 25 km grid cells) [*Cavalieri et al.*, 2008]. This dataset has been extensively compared with both sea ice concentrations derived from LandSat imagery [*Emery et al.*, 1994], *AVHRR* [*Comiso et al.*, 1997]), and operational ice charts in the Canadian Archipelago [*Agnew and Howell*, 2003]. These previous studies show SSMR/SSMI underestimates the sea ice extent in the melt and refreeze season by ~5%, and that uncertainties in concentration can reach 20%. Nonetheless, cross-evaluation of sea ice concentrations retrieved from SSM/I against high-resolution IMS data and MODIS imagery, shows that the use of SSM/I in the nearshore zone of the Drew Point area along the Beaufort Sea is adequate for assessment of the

[1]INSTAAR, University of Colorado at Boulder, Boulder, Colorado, USA.
[2]Department of Geological Sciences, University of Colorado at Boulder, Boulder, Colorado, USA.
[3]Stratus Consulting, Inc., Boulder, Colorado, USA.
[4]CIRES, University of Colorado at Boulder, Boulder, Colorado, USA.
[5]U.S. Geological Survey, Lakewood, Colorado, USA.

Copyright 2011 by the American Geophysical Union.
0094-8276/11/2011GL048681

longterm trends in break-up and freeze-up days (auxiliary material).[1]

[5] We assume a threshold sea ice concentration of 15% to represent the sea ice margin, following previous sea ice margin definitions [*Meier and Stroeve*, 2008]. Sensitivity analysis shows use of a different threshold, for example a 50% ice concentration [*Swail et al.*, 2006], results in similar data trends to those presented here. In the study zone, all days with SIC < 15% are considered "open water", in the sense that waves are not damped by sea ice cover. We employ an edge detection algorithm to map the regional sea ice margin for any given day, allowing calculation of the distance from the sea ice margin cells to our coastal cells with a great circle distance algorithm.

[6] We focused our analysis on three adjacent coastal grid-cells, covering a reach of ~75 km near our field study area. Each individual coastal cell can be influenced by brightness temperature 'contamination' from the nearby land included in the swaths. This effect could potentially lead to overestimation of sea ice in the nearshore region. Our choice of three adjacent cells is designed to minimize this effect; as these three cells all have slightly different coastal geometry, and therefore slightly different land spill-over effects, we can assess the role of such contamination.

2.2. Wind Climate

[7] Wind was measured locally at Drew Point from August 2004 onwards. A longer time-series of wind observations is available from the meteorological station of Barrow, Alaska (1979–2007), located about 110 km west of Drew Point. Hourly wind speeds and directions of the two stations correlate well for the overlapping 3 years, especially if we employ a lag to compensate for the time required for storms to travel from Barrow to Drew Point. Wind speeds at Drew Point lag ~2 hours behind winds at Point Barrow during the open water season. We deemed wave-generating wind events (>5 m s^{-1}) to be most relevant for wave modeling. For all years prior to 2004, we calculate local windspeed at Drew Point, U_{DP}, based on the Barrow station data, U_{BRW}, corrected with the transfer function obtained for only those events ($U_{DP} = 0.95U_{BRW} + 0.37$, $r^2 = 0.8$).

2.3. Bathymetry

[8] The bathymetry along our study reach, bounded by a straight stretch of the Beaufort Coast, is nearly uniform in the along-shore direction, and slopes gently offshore at ~1 m km^{-1} [*Ricketts*, 1953; *Greenberg et al.*, 1981]. This linear, uniform, geometry justifies a 1D shallow-water wave modeling approach; we acknowledge that any 1D approach ignores wave refraction when winds are not shore-normal. Our 2009 bathymetric survey indicates that water depth immediately offshore ranges 0.5–2.5 m. We modeled wave heights for water depths ranges 0.5–6.0 m; and present results for 2 m water depth. We ignore the effect of tides, as the mean range of tide is very low (0.08–0.15 m for stations at Point Barrow and Prudhoe Bay [*Hopper*, 2007]).

2.4. Shallow-Water, Fetch-Limited Waves

[9] In our model, the observed wind direction determines hourly fetch, i.e., the distance of the SSMI-determined sea ice margin to the coast in the direction from which the wind is blowing. A minimum fetch of 3 km is defined for times when winds originate from shoreward directions. For a given wind speed Ua (m s^{-1}), and fetch F (m), significant wave height H (m), in shallow water of depth d (m), can be approximated as follows [*U.S. Army Corps of Engineers*, 1984]:

$$\frac{gH}{Ua^2} = 0.283\tanh\left(0.53\left(\frac{gd}{Ua^2}\right)^{\frac{3}{4}}\right)\tanh\left\{\frac{0.00565\left(\frac{gF}{Ua^2}\right)^{\frac{1}{2}}}{\tanh\left[0.530\left(\frac{gd}{Ua^2}\right)^{\frac{3}{8}}\right]}\right\} \quad (1)$$

where g is the acceleration due to gravity. The adjusted wind speed Ua, depends on the windspeed, U_{10m}, at 10 m height:

$$Ua = 0.71U_{10m}^{1.23} \quad (2)$$

As this relationship requires wind speeds at 10 m, we convert the observed wind speed at 3 m height, U_{3m}, to the windspeed, U_{10m}, at 10 m height, assuming a neutrally buoyant atmosphere in which the law of the wall holds:

$$U_{10m} = U_{3m}(\log(10/z_0)/\log(3/z_0)) \quad (3)$$

with z_0 = 0.06 m; this roughness height is representative of large open water surfaces [*Brutsaert*, 1984].

[10] These calculations result in a time series of predicted hourly wave heights over the entire open water season, from the first day of open water (F-OW) to the last day of open water (L-OW). Our model does not account for storm surge, which can both set up or set down the water level, implying that the total exposure of a coastal bluff to accumulated wave height over the entire open water season, W, is simply a first-order proxy for thermal erosion:

$$W = \int_{F-OW}^{L-OW} Hdt \quad (4)$$

3. Thirty Years of Coastal Change

[11] Passive Microwave data allows analysis of 30 years of daily sea ice concentrations at locations around the Arctic Ocean coast. Open water season near our studied stretch of Beaufort Sea coastline has undergone a profound change over the last 30 years (Figure 1). Coastal sea ice moves out about three weeks earlier now than 30 years ago (day 204 vs. day 224), and sea ice moves back in about one month later now than 30 years ago (day 300 vs. day 269) (Figure 1, top). The duration of the open water season has therefore more than doubled from ~45 days to ~95 days. On average, the open water season extends by 17.5 days per decade, with more of that extension occurring into the fall.

[12] The Beaufort Sea region has experienced some of the fastest rates of sea ice cover change in the entire Arctic [*Shirasawa et al.*, 2009]; open water duration has increased as fast as 11 days $decade^{-1}$ [*Markus et al.*, 2009]. Our analysis therefore reveals a 50% greater rate of change of the open water season near the coast than in the Beaufort Sea as a whole. This suggests that changes at or near the coast may locally outpace the larger regional Arctic Ocean pattern of melt and sea ice decline, with potentially far-reaching

[1]Auxiliary materials are available in the HTML. doi:10.1029/2011GL048681.

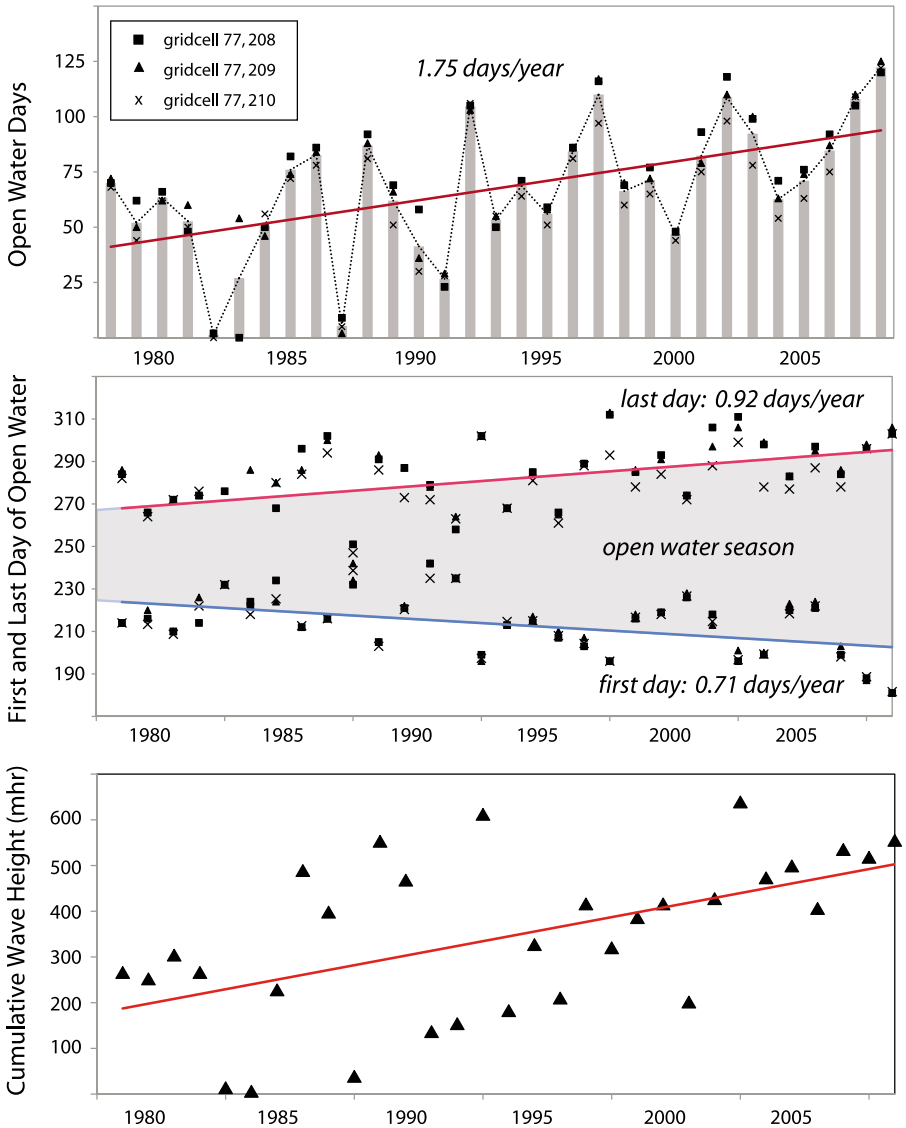

Figure 1. (top) Number of Open Water Days for ~75 km coastal zone along Beaufort Sea, 1979–2009. (middle) First Day of Open Water (blue) and Last Day of Open Water (red), 1979–2009. (bottom) Modeled integrated wave height over open water seasons, 1979–2009.

implications for changes in coastlines and nearshore ecosystems, as well as development, navigational and port activities.

[13] It is important to note that the open water season in our study area extends more rapidly toward the fall (September and October~0.92 day yr^{-1}) than toward the early summer (July~0.71 days yr^{-1}) (Figure 1, middle). This asymmetry in change has been observed in atmospheric warming [*Serreze et al.*, 2009] and Arctic-wide sea ice analyses [*Markus et al.*, 2009], and has been attributed to the fact that early melt allows the ocean water a longer period to warm up, and that retention of this heat into the fall delays freeze-up. In the Beaufort Sea, more storms occur in the fall than in the summer; over the period 1950 to 2000, an average of 8.5 storms (here defined as having wind speeds exceeding 10 m s^{-1} for 48 hours) occurred in September and October, while an average of 6.5 storms occurred in the months of July and August [*Atkinson*, 2005].

[14] In Figure 1 (bottom) we present the integrated wave height over the open water season, *W*, for the thirty-year monitoring period, which serves as an annual proxy for coastal erosion caused by waves lapping onto the bluffs. Although inter-annual variability is high, our data shows a temporal trend of increasing integrated wave height, increasing by two-and-half fold over 30 years (Figure 1, bottom).

4. Short Term Observations of Coastal Change

[15] To supplement our modeling predictions, we use time-lapse photography and field data from a 3 km transect at Drew Point, approximately halfway between Point Barrow and Prudhoe Bay, AK. Time-lapse images were collected at two coastal sites every two hours between June 20 and August 2, 2008 (day 172–215; see Movie S1 in the auxiliary material), allowing detailed reconstruction of bluff erosion histories as well as snapshots of actual wave heights to compare with modeling predictions [*Wobus et al.*, 2011]. Permafrost bluffs along this stretch of coast are ~5 m high. Analyses of 16 bluff samples indicate that frozen bluffs

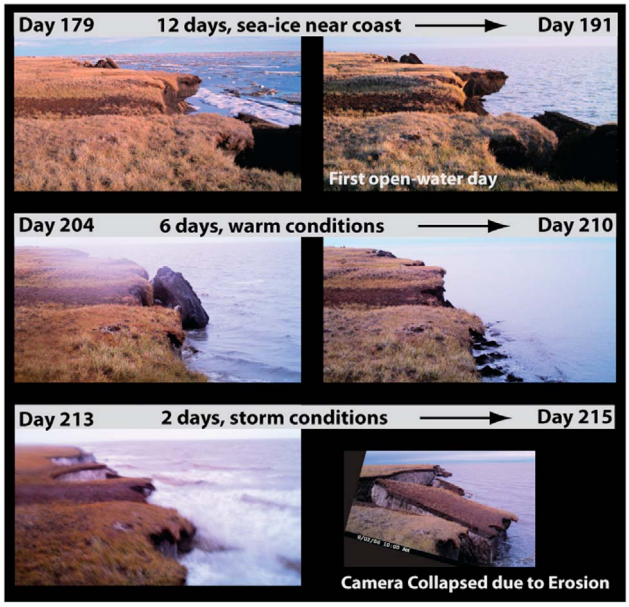

Figure 2. Images from time-lapse camera at Drew Point, along the Beaufort Coast illustrate three different regimes. (top) Limited coastal erosion occurs from day 179–191 when sea ice still protects the coast. (middle) Toppled block erodes rapidly from day 204–210 under warm summer conditions. (bottom) Rapid bluff failure in mid-summer storm.

comprise on average 64% ice by mass (Table S1 in the auxiliary material). The bluffs therefore have high mechanical strength, but limited resistance to thermal erosion processes due to high interstitial ice content.

[16] Figure 2 shows a sequence of time-lapse images over the summer of 2008. On day 179, land-fast sea ice is still present at Drew Point, although it is already covered with shallow melt-water puddles. The last few floating chunks of ice can be observed from the time-lapse imagery on days 189 and 190. Day 191 is the first day without any floating sea-ice, a full open-water day. By comparison, the remotely-sensed sea ice concentration falls below 15% on day 191 in the ~20 km wide coastal region around Drew Point and on days 187 and 189 in the adjacent cells. This confirms the accuracy of the remotely-sensed regional sea ice concentration as a measure of the conditions in the near-coastal zone, and the choice of 15% SIC as a threshold. During the period in which sea ice is still present, bluff erosion occurs through only subaerial melt due to air temperatures that reached 12°C. However, rates of subaerial melt are very low, measured erosion being limited to 10–20 cm total over the period of shorefast ice (day 179 to 191) (Figure 2).

[17] Once sea ice has disappeared, the lower parts of the icy bluffs become thermally notched by small waves even during fair weather conditions. Blocks are eventually undercut, fail commonly along ice wedges, and fall into the shallow coastal water. Once fallen, they melt within a few days (e.g., on day 204 a large failure happens and the ~4 m block has completely disappeared by day 210). The time-lapse images show wave heights of <30 cm during this period. Even at the beginning of the ice-free season, fetch is not necessarily a limiting factor; under common E-NE wind directions, more than 700 km of open water exists (Figure 3c). Winds blowing from the land cause temporarily sharp drops in fetch. During early open-water season, days 191–202, there were no substantial storm events and the erosion is entirely thermally-controlled; mechanical wave energy plays little to no role.

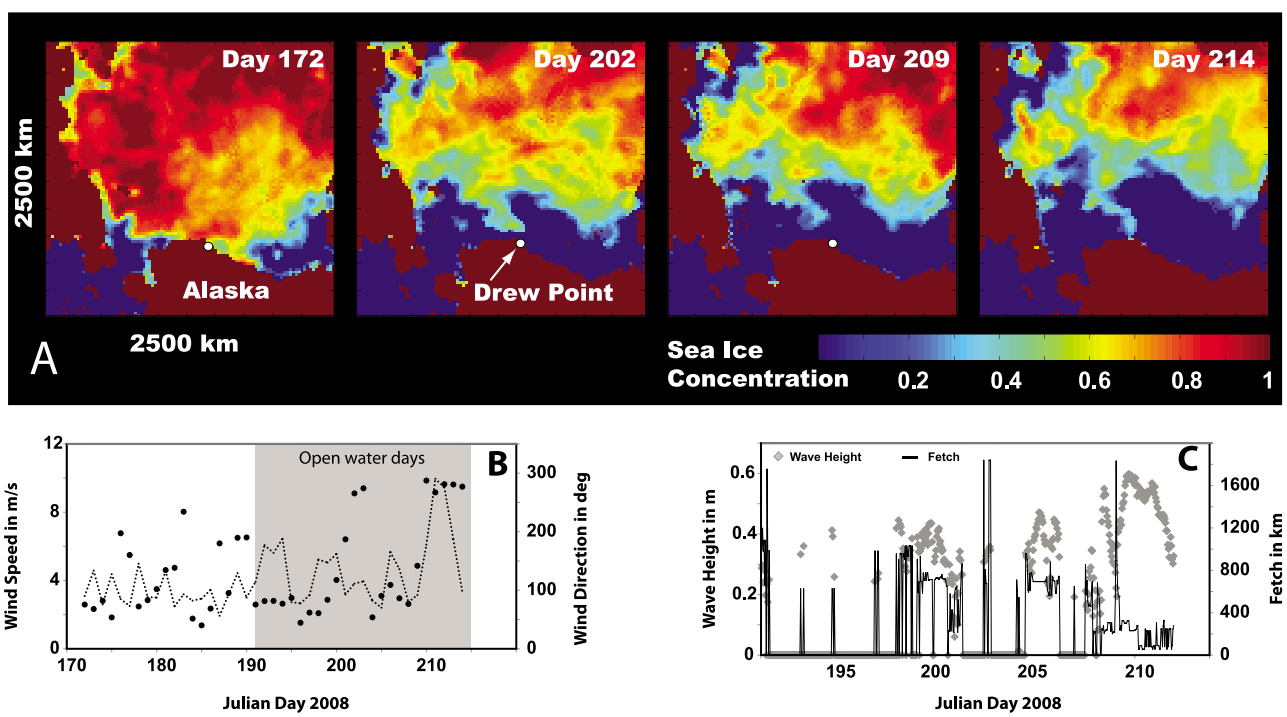

Figure 3. (a) Regional sea ice concentrations (SIC) as mapped with Nimbus 7-SMMR/SSM/I and DMSP SSMI Passive Microwave data for days 172–day 214, 2008. (b) Wind speed and wind direction observed at Drew Point for days 172–214, 2008. (c) Modeled hourly fetch and wave height at 2 m water depth for open water days 191–214, 2008.

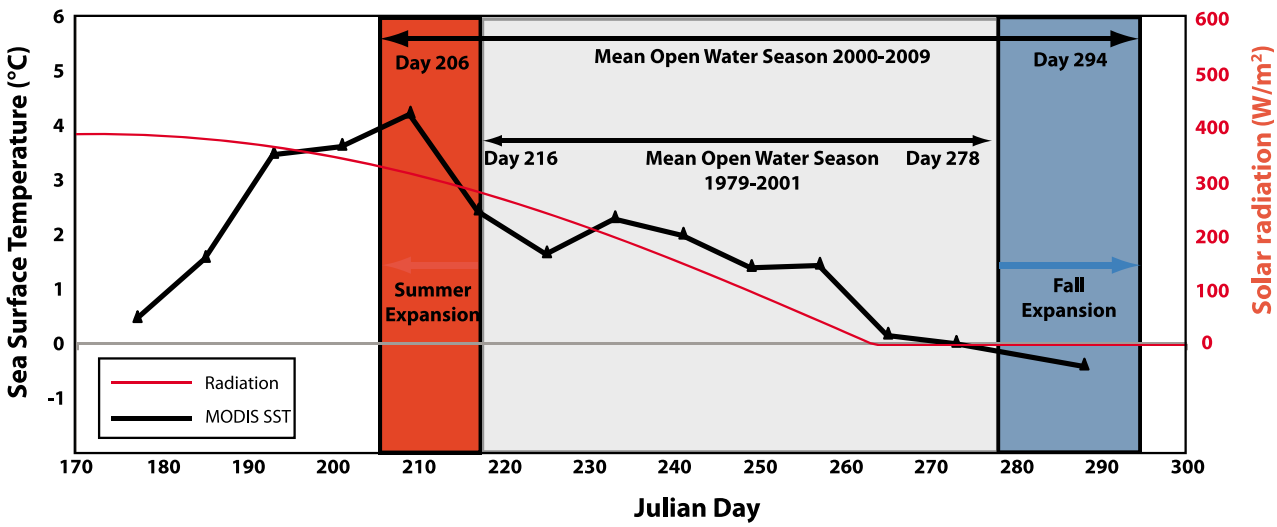

Figure 4. Mean Sea Surface Temperature (2000–2009) versus the day in the year (black line). Sea surface temperature is determined based on MODIS-calibrated mid- and far-IR radiances. The envelops of the mean open water season for 1979–2001 and 2000–2009 show significant expansions in both the summer and fall season, but notably the SST is much higher during the month of July, when insolation is higher (red line). This implies that thermal erosion may be more efficient during that time of the open water season.

[18] Over the last few days of the recording interval (days 210–215), a WNW storm occurred, with air temperature dropping to ~2°C and wind speed exceeding 10 m s^{-1} over 48 hours. During this period, sea surface temperatures determined for 4.6 km gridcells based on MODIS-calibrated mid- and far-IR radiances [*Walton et al.*, 1998] were 3.5–4.2°C. Meteorological observations within 30–150 m of the bluffs indicate even higher air temperatures of 8–10°C in early August [*Wobus et al.*, 2011]. Fetch predicted from the sea ice edge mapping is limited to <200 km due to the presence of a tongue of sea ice in WNW sector of the Beaufort Sea (Figure 3a). We observe the highest waves splashing the bluffs, as well as storm setup. While wave heights qualitatively inferred from our time-lapse photography sequence were up to 0.4–0.5 m, it appears that the bluff faces get efficiently washed free of sediment by breaking waves and storm surge to higher levels. Modeled wave heights for this storm are between 0.5–0.6 m (Figure 3c). While we do not have water level observations for this specific storm, set up due to storm surge in August 2009 and 2010 under similar wind stress regimes amount to 0.4 m nearshore, effectively doubling the bluff height subjected to thermal erosion. While this storm lasts only 3 days, and represents only 13% of the monitored open water season, the storm represents 46% of the integrated wave height over the monitoring period. Extensive bluff notching and block failures occurred during this storm (Figure 2). The combination of significant water access to the bluff face and relatively warm sea water temperatures indicate that this type of storm could be responsible for a large fraction of the thermal erosion that occurs along this type of permafrost coastline.

5. Discussion and Conclusions

[19] Wave height integrated over the open water seasons, *W*, of 1979–2009 increased dramatically (Figure 1, bottom). In addition to 2009, the five years with the largest integrated wave heights over the open water season were 2003, 1993, 2008, 1989 and 2007 (Figure 1, bottom). While 2007 had the lowest sea ice minimum extent over the region, according to our modeling, the integrated wave height was not at its 30 year maximum. This result points to the greater importance of storms than of fetch. Even if the sea ice margin is very far from shore, storms are needed to generate waves and setup to bathe the bluffs in the warm water that in turn enhances melt rates.

[20] Using our model results, we can average the annual integrated wave heights for the periods over which mean annual coastal erosion rates have been calculated from mapping (see Table S2 in the auxiliary material). *Jones et al.* [2009] estimated mean coastal erosion rates of 8.7 m yr^{-1} for 1979–2002, compared to 13.6 m yr^{-1} for 2002–2007 along the Beaufort Sea – a factor of ~1.6 increase. The number of open water days increased by a similar factor of approximately 1.5 (~63 days for 1979–2002 vs. ~96 days for 2002–2007).

[21] The above comparisons indicate that open water days may be a good first-order predictor of coastal erosion. However, both the integrated annual fetch and integrated wave height increased at slightly greater rates than did erosion rates over this time period (a factor of ~1.8 increase (Table S2 in the auxiliary material)). We hypothesize that the over-estimation of the acceleration based upon these latter proxies is associated with asymmetry of the wave climate, which is more intense in the fall. Erosion of the Drew Point bluffs is rapid even during relatively calm ocean conditions, and is therefore also governed by seawater temperatures, which peak in early August and then decline during the fall (Figure 4). The increased storm activity in the fall [*Atkinson*, 2005], as reflected in the modeled integrated wave height, may be countered by the lower ocean temperatures at that time. However, should the extension of ice-free conditions advance more strongly into the middle of summer, when insolation peaks (Figure 4), we suspect that sea surface temperatures will warm even faster and hence erosion may accelerate yet more strongly. To test more fully

these hypotheses and to make regional quantitative predictions of coastal erosion, rigorous treatment of both the thermal evolution of the ocean, and of storm surges on which the waves of storms ride are critical next steps.

[22] **Acknowledgments.** The authors thank T. Mefford, NOAA; W. Meier, NSIDC; and C. Sherwood, USGS. for data and model discussions. This project is funded by the National Oceanographic Partnership Program (Award N00014-07-1-1017).

[23] The Editor thanks Gwyn Lintern for assistance in evaluating this paper.

References

Agnew, T., and S. Howell (2003), The use of operational ice charts for evaluating passive microwave ice concentration data, *Atmos. Ocean*, *41*, 317–331, doi:10.3137/ao.410405.

Are, F., E. Reimnitz, M. Grigoriev, H. Hubberten, and V. Rachold (2008), The influence of cryogenic process on the erosional arctic shoreface, *J. Coastal Res.*, *241*, 110–121.

Atkinson, D. E. (2005), Observed storminess patterns and trends in the circum-Arctic coastal regime, *Geo Mar. Lett.*, *25*, 98–109, doi:10.1007/s00367-004-0191-0.

Brutsaert, W. (1984), *Evaporation into the Atmosphere: Theory, History and Applications*, 299 pp., D. Reidel, Dordrecht, Netherlands.

Cavalieri, D., C. Parkinson, P. Gloersen, and H. J. Zwally (2008), Sea ice concentrations from Nimbus-7 SMMR and DMSP SSM/I passive microwave data, digital media, Natl. Snow and Ice Data Cent., Boulder, Colo.

Clow, G. D. (2008), USGS polar temperature logging system, description and measurement uncertainties, *U.S. Geol. Surv. Tech. Methods*, *2-E3*, 24 pp.

Comiso, J. C., J. D. Cavalieri, C. L. Parkinson, and P. Gloersen (1997), Passive microwave algorithms for sea ice concentration: A comparison of two techniques, *Remote Sens. Environ.*, *60*, 357–384, doi:10.1016/S0034-4257(96)00220-9.

Emery, W. J., C. Fowler, and J. Maslanik (1994), Arctic sea ice concentrations from special sensor microwave imager and advanced very high resolution radiometer satellite data, *J. Geophys. Res.*, *99*(C9), 18,329–18,342, doi:10.1029/94JC01413.

Greenberg, J., P. E. Hart, and A. Grantz (1981), Bathymetric map of the continental shelf, slope and rise of the Beaufort Sea North of Alaska, scale 1:500,000, *U.S. Geol. Surv. Misc. Invest.*, *1182-A*.

Holland-Bartels, L., and B. Pierce (Eds.) (2011), An evaluation of the science needs to inform decisions on Outer Continental Shelf energy development in the Chukchi and Beaufort Seas, Alaska, *U.S. Geol. Surv. Circ.*, *1370*, 278 pp.

Hopper, M. (2007), *Manual of Harmonic Analysis and Prediction of Tides*, *Special Publ.*, vol. 98, U.S. Gov. Print. Off., Washington, D. C.

Hoque, M. A., and W. H. Pollard (2009), Arctic coastal retreat through block failure, *Can. Geotech. J.*, *46*, 1103–1115, doi:10.1139/T09-058.

Jones, B. M., C. D. Arp, M. T. Jorgenson, K. M. Hinkel, J. A. Schmutz, and P. L. Flint (2009), Increase in the rate and uniformity of coastline erosion in Arctic Alaska, *Geophys. Res. Lett.*, *36*, L03503, doi:10.1029/2008GL036205.

Kobayashi, N. (1985), Formation of thermoerosional niches into frozen bluffs due to storm surges on the Beaufort Sea coast, *J. Geophys. Res.*, *90*(C6), 11,983–11,988, doi:10.1029/JC090iC06p11983.

Lantuit, H., and W. H. Pollard (2008), Fifty years of coastal erosion and retrogressive thaw slump activity on Herschel Island, southern Beaufort Sea, Yukon Territory, Canada, *Geomorphology*, *95*(1–2), 84–102, doi:10.1016/j.geomorph.2006.07.040.

Markus, T., J. Stroeve, and J. Miller (2009), Recent changes in Arctic sea ice melt onset, freezeup, and melt season length, *J. Geophys. Res.*, *114*, C12024, doi:10.1029/2009JC005436.

Mars, J. S., and D. W. Houseknecht (2007), Quantitative remote sensing study indicates doubling of coastal erosion rate in past 50 yr along a segment of the Arctic coast of Alaska, *Geology*, *35*, 583–586, doi:10.1130/G23672A.1.

Meier, W., and J. Stroeve (2008), Comparison of sea-ice extent and ice-edge location estimates from passive microwave and enhanced-resolution scatterometer data, *Ann. Glaciol.*, *48*, 65–70, doi:10.3189/172756408784700743.

Ping, C. L., G. J. Michaelson, L. Guo, M. T. Jorgenson, M. Kanevskiy, Y. Shur, and F. Dou (2011), Soil carbon and material fluxes across the eroding Alaska Beaufort Sea coastline, *J. Geophys. Res.*, *116*, G02004, doi:10.1029/2010JG001588.

Ricketts, M. G. (1953), Hydrographic survey, *Rep. ARW-4251*, U.S. Coast and Geod. Surv., Washington, D. C.

Serreze, M. C., J. E. Walsh, F. S. Chapin III, T. Osterkamp, M. Dyurgerov, V. Romanovsky, W. C. Oechel, J. Morison, T. Zhang, and R. G. Barry (2000), Observational evidence of recent change in the northern high-latitude environment, *Clim. Change*, *46*, 159–207.

Serreze, M. C., M. Holland, and J. Stroeve (2007), Perspectives on the Arctic's shrinking sea-ice cover, *Science*, *315*, 1533–1536, doi:10.1126/science.1139426.

Serreze, M. C., A. P. Barrett, J. C. Stroeve, D. N. Kindig, and M. M. Holland (2009), The emergence of surface-based Arctic amplification, *Cryosphere*, *3*, 11–19, doi:10.5194/tc-3-11-2009.

Shirasawa, K., H. Eicken, K. Tateyama, T. Takatsuka, and T. Kawamura (2009), Sea-ice thickness variability in the Chukchi Sea, spring and summer 2002–2004, *Deep Sea Res., Part II*, *56*, 1182–1200, doi:10.1016/j.dsr2.2008.10.015.

Smith, S. L., V. E. Romanovsky, A. G. Lewkowicz, C. R. Burn, M. Allard, G. D. Clow, K. Yoshikawa, and J. Throop (2010), Thermal state of permafrost in North America: A contribution to the International Polar Year, *Permafrost Periglacial Processes*, *21*, 117–135, doi:10.1002/ppp.690.

Solomon, S. M., D. L. Forbes, and B. Kierstead (1994), Coastal impacts of climate change: Beaufort Sea erosion study, *Geol. Surv. Can. Open File*, *2890*, 85 pp.

Steele, M., W. Ermold, and J. Zhang (2008), Arctic Ocean surface warming trends over the past 100 years, *Geophys. Res. Lett.*, *35*, L02614, doi:10.1029/2007GL031651.

Stroeve, J., A. Frei, J. McCreight, and D. Ghatak (2008), Arctic sea-ice variability revisited, *Ann. Glaciol.*, *48*(1), 71–81, doi:10.3189/172756408784700699.

Swail, V. R., V. J. Cardone, M. Ferguson, D. J. Gummer, E. L. Harris, E. A. Orelup, and A. T. Cox (2006), The MSC50 wind and wave reanalysis, paper presented at the 9th International Workshop On Wave Hindcasting and Forecasting, *Environ. Can.*, Victoria, B. C., 25–29 Sept.

U.S. Army Corps of Engineers (1984), *Shore Protection Manual*, vol. 1, 4th ed., 1088 pp., Dep. of the Army, Vicksburg, Miss.

Walton, C. C., W. G. Pichel, and J. F. Sapper (1998), The development and operational application of nonlinear algorithms for the measurement of sea surface temperatures with the NOAA polar-orbiting environmental satellites, *J. Geophys. Res.*, *103*(C12), 27,999–28,012, doi:10.1029/98JC02370.

Wobus, C., R. S. Anderson, I. Overeem, N. Matell, G. Clow, and F. Urban (2011), Thermal erosion of a permafrost coastline: Improving process-based models using time-lapse photography, *Arct. Antarct. Alp. Res.*, in press.

R. S. Anderson, N. Matell, and I. Overeem, INSTAAR, University of Colorado at Boulder, 1560 30th St., Boulder, CO 80303, USA. (irina.overeem@colorado.edu)

G. D. Clow and F. E. Urban, U.S. Geological Survey, Box 25046, Mail Stop 980, Lakewood, CO 80225, USA.

C. W. Wobus, Stratus Consulting, Inc., 1881 Ninth St., Boulder, CO 80302, USA.